



ARL-TR-9644 • FEB 2023



An Efficient, One-Step Synthesis of 2,4,6-Triaminobenzene-1,3,5-tricarboxylaldehyde

**by David C McLeod, Kätchen K Lachmayr, John Biswakarma,
Adam Switek, Robert H Lambeth, and Steven R Lustig**

Approved for public release: distribution unlimited.

NOTICES

Disclaimers

The findings in this report are not to be construed as an official Department of the Army position unless so designated by other authorized documents.

Citation of manufacturer's or trade names does not constitute an official endorsement or approval of the use thereof.

Destroy this report when it is no longer needed. Do not return it to the originator.



An Efficient, One-Step Synthesis of 2,4,6-Triaminobenzene-1,3,5-tricarboxylaldehyde

David C McLeod and Robert H Lambeth

DEVCOM Army Research Laboratory

**Kätchen K Lachmayr, John Biswakarma, Adam Switek, and
Steven R Lustig**

Northeastern University

REPORT DOCUMENTATION PAGE				Form Approved OMB No. 0704-0188	
<p>Public reporting burden for this collection of information is estimated to average 1 hour per response, including the time for reviewing instructions, searching existing data sources, gathering and maintaining the data needed, and completing and reviewing the collection information. Send comments regarding this burden estimate or any other aspect of this collection of information, including suggestions for reducing the burden, to Department of Defense, Washington Headquarters Services, Directorate for Information Operations and Reports (0704-0188), 1215 Jefferson Davis Highway, Suite 1204, Arlington, VA 22202-4302. Respondents should be aware that notwithstanding any other provision of law, no person shall be subject to any penalty for failing to comply with a collection of information if it does not display a currently valid OMB control number.</p> <p>PLEASE DO NOT RETURN YOUR FORM TO THE ABOVE ADDRESS.</p>					
1. REPORT DATE (DD-MM-YYYY) February 2023		2. REPORT TYPE Technical Report		3. DATES COVERED (From - To) 1 December 2021 – 30 June 2022	
4. TITLE AND SUBTITLE An Efficient, One-Step Synthesis of 2,4,6-Triaminobenzene-1,3,5-tricarboxylaldehyde				5a. CONTRACT NUMBER	
				5b. GRANT NUMBER W911NF2020024	
				5c. PROGRAM ELEMENT NUMBER	
6. AUTHOR(S) David C McLeod, Kätchen K Lachmayr, John Biswakarma, Adam Switek, Robert H Lambeth, and Steven R Lustig				5d. PROJECT NUMBER	
				5e. TASK NUMBER	
				5f. WORK UNIT NUMBER	
7. PERFORMING ORGANIZATION NAME(S) AND ADDRESS(ES) DEVCOM Army Research Laboratory ATTN: FCDD-RLA-MA Aberdeen Proving Ground, MD 21005				8. PERFORMING ORGANIZATION REPORT NUMBER ARL-TR-9644	
9. SPONSORING/MONITORING AGENCY NAME(S) AND ADDRESS(ES)				10. SPONSOR/MONITOR'S ACRONYM(S)	
				11. SPONSOR/MONITOR'S REPORT NUMBER(S)	
12. DISTRIBUTION/AVAILABILITY STATEMENT Approved for public release: distribution unlimited.					
13. SUPPLEMENTARY NOTES ORCID IDs: David C McLeod, 0000-0001-5293-6060; Robert H Lambeth, 0000-0001-7664-015X					
14. ABSTRACT This report details the synthesis, isolation, and characterization of a hexa-functional monomer, 2,4,6-triaminobenzene-1,3,5-tricarboxylaldehyde, which consists of a single benzene ring with three pendant aldehyde groups alternating with three free amine groups. This compact, symmetrical monomer may be especially useful to produce dense, triangular-lattice, imine-based 2D polymers such as graphimine, or as a starting material for other high-value, nitrogen-rich chemicals such as pharmaceuticals and energetic compounds.					
15. SUBJECT TERMS imine, amine, aldehyde, monomer, covalent organic framework, 2D polymer, Sciences of Extreme Materials					
16. SECURITY CLASSIFICATION OF:			17. LIMITATION OF ABSTRACT UU	18. NUMBER OF PAGES 37	19a. NAME OF RESPONSIBLE PERSON David C McLeod
a. REPORT Unclassified	b. ABSTRACT Unclassified	c. THIS PAGE Unclassified			19b. TELEPHONE NUMBER (Include area code) 410-306-4943

Contents

List of Figures	iv
List of Tables	v
1. Introduction	1
2. Experimental Methods	2
3. Analytical Techniques and Characterization	4
4. Results and Discussion	5
4.1 Reaction Mechanism	5
4.2 Characterization of Products	6
4.3 Isolation and Stability of the Monomer	10
5. Conclusions and Future Directions	13
6. References	14
Appendix. Supplementary Information	16
List of Symbols, Abbreviations, and Acronyms	29
Distribution List	30

List of Figures

Fig. 1	Synthesis of 2,4,6-triaminobenzene-1,3,5-tricarboxylaldehyde, 2, from Rubin's aldehyde, 1, using anhydrous ammonia in dimethyl sulfoxide (DMSO)	2
Fig. 2	Reaction apparatus setup (A) and active reaction (B)	3
Fig. 3	Arrow-pushing reaction mechanism for NAS of ammonia with 1 (A), and the experimentally unobserved aldehyde amination (B).....	6
Fig. 4	¹ H NMR of 2 (A) and 1 (B) using 500-MHz spectrometer in DMSO- <i>d</i> ₆	7
Fig. 5	¹³ C NMR of 2 (A) and 1 (B) using 400-MHz spectrometer in DMSO- <i>d</i> ₆	7
Fig. 6	FTIR spectra of Rubin's aldehyde (1), TABTCA (sample kl01-112-B) (2), and cross-linked TABTCA (sample kl01-91-solid) (3), with selected peaks and functional group assignment	8
Fig. 7	PXRD of 3 (sample kl01-91-cross-linked) showing an absence of crystallinity	9
Fig. 8	TGA of 2	10
Fig. 9	¹³ C NMR collected with a 500-MHz spectrometer of 1 (A), 2 prepared through precipitation in water (B), 1 M HCl (C), and 9.25 M HCl (D) in DMSO- <i>d</i> ₆	11
Fig. 10	¹³ C NMR collected with a 500-MHz spectrometer of 2 prepared through precipitation in 1 M acetic acid, in DMSO- <i>d</i> ₆	12
Fig. A-1	Reaction scheme showing the conversion of 1 to 2,4,6-tris(iminomethyl)benzene-1,3,5-triamine, through the addition of six ammonia molecules and removal of three water and three HBr molecules (A). Reaction is predicted, via molecular mechanics, to be exothermic and favored with a very negative Gibbs energy of reaction (B).	17
Fig. A-2	¹ H NMR of products removed from dichloromethane (DCM) washing of crude product 2, collected on a 500-MHz spectrometer using dimethyl sulfoxide (DMSO)- <i>d</i> ₆	18
Fig. A-3	Compound 2 collected in at the bottom of a fritted funnel	18
Fig. A-4	Photographs of a mixture of 2 and 3. A neat reaction solution producing 2 was allowed to dry under air for 3 days, resulting in a layer effect of 2 on the bottom surface sandwiched between glass and a top layer of 3 that was exposed to air (A). NMR tubes contain a DMSO solution of a 2 and 3 mixture, where 2 is soluble in DMSO, producing a yellow solution, and 3 is insoluble, forming a brown solid at the bottom of the left tube (B).....	18

Fig. A-5	Initial crude reaction solution of compound 2 (A), which was the precipitated in water, 1 M HCl, and 9.25 M HCl (B) to analyze amine-salt formation and stabilization of 2.....	19
Fig. A-6	Concentration of the crude reaction solution containing 2 in DMSO to 70 °C under high vacuum results in the formation of a gel-like substance (A). This gel was isolated and washed with fresh DMSO (B) and re-solubilization in DMSO was attempted (C) to recover unreacted 2, with poor results. Drying under high vacuum to remove DMSO resulted in 3 as a powdered substance (D) that appears soluble in trifluoroacetic acid. The powder has no proton resonances (E), but has Fourier transform infrared (FTIR) spectra consistent with other 3 that were formed without prior gelation.	19
Fig. A-7	Comparison of neutral (2) and charged structures (4)	20

List of Tables

Table A-1	DFT-derived frequencies, scale frequencies, intensities, and selected animation descriptions for 4.....	20
Table A-2	Comparison of select computational DFT data from 4 to experimental data on compound kl01-112-B. Intensities are in percent transmittance for experimental data.	22
Table A-3	Comparison of select computational DFT data from 4 to experimental data on compound kl01-91-monomer. Intensities are in percent transmittance for experimental data.....	24
Table A-4	DFT-derived frequencies, scale frequencies, intensities, and selected animation descriptions for 2.....	26
Table A-5	Comparison of select computational DFT data from 2 to experimental data on compound kl01-122-B. Intensities are in percent transmittance for experimental data.	27
Table A-6	Comparison of select computational DFT data from 2 to experimental data on compound kl01-91-monomer. Intensities are in percent transmittance for experimental data.....	28

1. Introduction

Substituted benzene rings, particularly those with pendant functional groups arranged in a symmetrical manner, are especially useful as rigid building blocks in the synthesis of covalent organic frameworks (COFs). The synthesis of imine-based COFs typically involves the reaction of a monomer with multiple aryl amine groups with another monomer with multiple aryl aldehyde groups in the presence of an acid catalyst. The resulting condensation reaction forms imine linkages (Ar-N=CH-Ar) between the monomers, often resulting in hexagonal 2D lattices that stack on top of one another in an orderly manner. COF monomers that contain both aldehyde and amine groups on the same molecule are not known in the literature, probably because such molecules are inherently unstable/self-reactive, making them difficult to synthesize and isolate. Multifunctional monomers consisting of only a single benzene ring with both pendant aldehyde and amine groups would be especially interesting if they could be stabilized prior to reaction because they could form COFs with unusually dense, compact structures. Additionally, these molecules could be useful as starting materials in the synthesis of other high-value, nitrogen-rich chemicals such as pharmaceuticals and energetic compounds.

In a recent technical report,¹ we disclosed a procedure for synthesizing a new monomer, (2,4,6-tris((diphenylmethylene)amino)benzene-1,3,5-tricarbaldehyde), which consists of a single benzene ring with three pendant aldehyde groups alternating with three benzophenone imine groups. A strategy was envisioned whereby the monomer under acidic conditions would undergo a transimination reaction between the aldehyde and benzophenone imine groups on different molecules, releasing the benzophenone protecting group in the process, to render an interesting 2D polymer called “graphimine,” which has an unusually rigid, triangular pore topology. Initial attempts to polymerize this monomer were not successful, possibly due to steric hinderance by the benzophenone groups; however, in the presence of water it was found that this monomer will release benzophenone and form the free amine monomer, 2,4,6-triaminobenzene-1,3,5-tricarboxylaldehyde (TABTCA), which proved to be stable in powder form over a period of days.

TABTCA (hereafter referred to as **2**, as shown in Fig. 1) could prove to be a much more useful monomer for the synthesis of graphimine and other COFs than the benzophenone imine monomer, because without the benzophenone groups it has significantly less parasitic mass, is less sterically hindered, and the nitrogen atoms of free amines are likely to be far more reactive than those contained in the benzophenone imines. Unfortunately, synthesizing **2** via hydrolysis of the

benzophenone imine molecule is low yielding, and the synthesis of the benzophenone imine monomer itself is not trivial. An efficient, direct synthesis of **2** from an easily accessible starting material is therefore highly preferable.



Fig. 1 Synthesis of 2,4,6-triaminobenzene-1,3,5-tricarboxylaldehyde, **2**, from Rubin's aldehyde, **1**, using anhydrous ammonia in dimethyl sulfoxide (DMSO)

Herein, we report the successful one-step synthesis of **2** via nucleophilic aromatic substitution (NAS) of the bromine atoms on 2,4,6-tribromobenzene-1,3,5-tricarbaldehyde (also known as Rubin's aldehyde, **1**) with anhydrous ammonia in DMSO under dry and air-free conditions (Fig. 1). Optimal conditions and procedures for isolating **2** in good yield as a relatively stable solid are discussed. Characterization of the desired compound **2**, as well as undesired decomposition products and cross-linked materials, was chiefly performed using ^1H and ^{13}C nuclear magnetic resonance (NMR) spectroscopy and Fourier transform infrared (FTIR) spectroscopy, with comparison of the experimentally derived FTIR spectra to computationally derived IR frequencies.

2. Experimental Methods

In synthetic chemistry, ammonia is often avoided for direct amination for several reasons: 1) lack of reaction control through generation of more basic and reactive aniline species, 2) generation of undesired di- and triaryl amines, and 3) when metal catalysts are used, ammonia could displace necessary ligands, deactivating the catalytic species.² In this instance, only the first argument is valid among these concerns, since metal catalysts are not employed and the desired product will be a triaryl amine. However, unlike the classic example of aliphatic amine alkylation, where the nucleophilicity of the formed product is greater than the reactants (comparing the pK_a of ammonia vs. ethylamine vs. triethylamine, in the instance of a bromoethane amine alkylation); the pK_a of substituted aniline species is typically less than ammonia (where aniline has a pK_a of 30.7 and 4-nitroaniline has a pK_a of 20.4), and further decreases with the presence of electron-withdrawing groups.^{3,4} Although the pK_a of **2** and its mono- and di-aminated counterparts are not yet known, it is reasonable to assume it is less than ammonia and will pose no nucleophilic competition to ammonia.

Recently, there has been considerable research into utilizing ammonia in chemical reactions, as it is typically an excellent “green” solvent for polar organic molecules and salts, is abundant and cheap, and is much easier to remove than typical polar aprotic solvents such as DMSO and *N,N*-dimethylformamide. With a boiling point of $-33\text{ }^{\circ}\text{C}$ and vapor pressure of 10 bar at $25\text{ }^{\circ}\text{C}$, liquid ammonia can be difficult to handle using standard synthetic organic chemistry techniques, especially at elevated temperature.⁵ DMSO has proven to be an excellent solvent for both compounds **1** and **2**. The solubility of ammonia in DMSO at $20\text{ }^{\circ}\text{C}$ is 2.6 g per 100 g of solvent.⁶ Like other polar organic solvents, it is expected that the solubility of the ammonia will decrease with an increase in temperature.⁷ Therefore, our approach uses a DMSO/ammonia reaction solution, where ammonia gas is bubbled through the reaction mixture, and then condensed back into the reaction mixture as a liquid using a Dewar-type condenser equipped with ethanol and dry ice, maximizing the exposure of ammonia to the reaction solution, as shown in Fig. 2A.

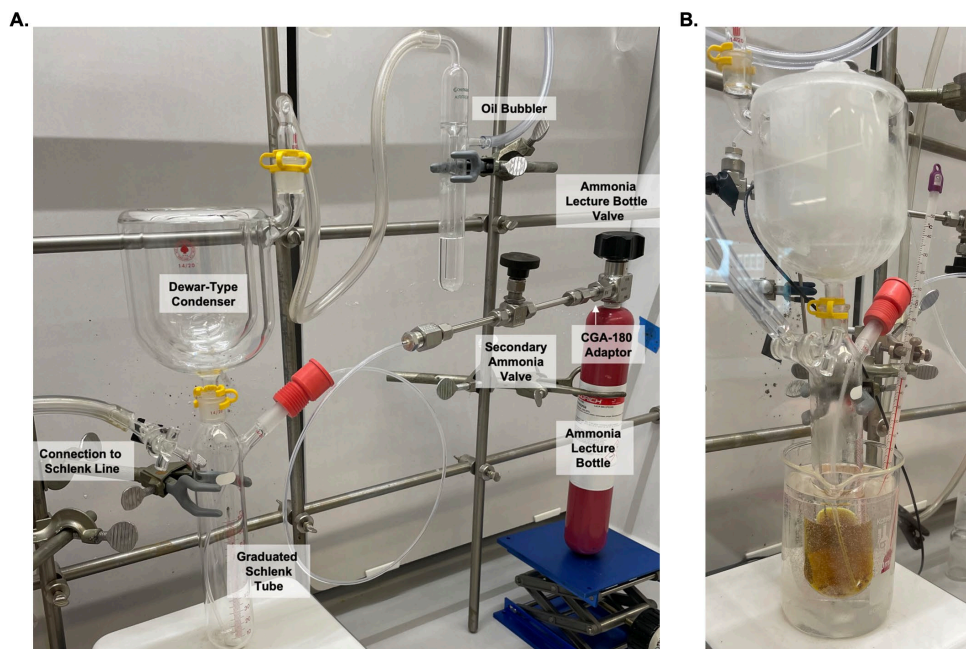


Fig. 2 Reaction apparatus setup (A) and active reaction (B)

Rubin’s aldehyde was prepared following the method described by Holst et al.⁸ Using a two-neck graduated Schlenk tube, 3 g (7.52 mmol) of **1** was dissolved in 50 mL of anhydrous DMSO using air-free techniques. The solution was brought to $50\text{ }^{\circ}\text{C}$, fully dissolving the Rubin’s aldehyde and producing a yellow color. The ammonia gas manifold was cycled three times between vacuum and nitrogen, and purged with nitrogen as the septa containing the flexible high-density polyethylene (HDPE) tubing was fitted to the ground-glass neck of the two-neck Schlenk tube. The end of the flexible HDPE tube remained above the solvent line until the

apparatus was fully assembled. The outlet of the Dewar-type condenser was exchanged from a penny-stopper to a hose adaptor connected to an oil bubbler, and an ethanol/dry ice bath was made within the body of the condenser. Once the ethanol/dry ice bath had reached $-40\text{ }^{\circ}\text{C}$, the flexible tubing was submerged to the bottom of the Schlenk tube, the ammonia valves were opened to allow for a moderate stream of ammonia bubbles into the reaction solution. The stopcock connecting the system to its supply of nitrogen was closed to allow the system to be purged with ammonia. Within 15 min the solution color changed from yellow to dark brown, and within 30 min liquid ammonia began to condense into the solution (Fig. 2B).

Once the ammonia had begun to condense, the nitrogen supply was opened to keep the system under slight positive pressure. The ammonia was delivered and condensed within the system for a period of 4 h. After 4 h, the ammonia valves were closed, the tube was lifted above the solvent line, and system was purged with nitrogen for 15 min. The weight of the ammonia lecture bottle was recorded to determine the amount delivered to the system (typically between 4.47 and 33.0 g of ammonia, corresponding to 0.26 and 1.94 mol, respectively, depending on bubbling rate). The reaction was then cooled to room temperature and precipitated in 150 mL of 1 M acetic acid solution, producing a yellow precipitate. The solution was then refrigerated for at least 1 day. The precipitate was collected via vacuum filtration and washed with ethanol to remove any trace water or acidic residue. To enhance the purity of the product and remove any traces of **1**, the crude product was washed with two 20-mL aliquots of dichloromethane (DCM) (typically less than 100 mg of DCM-soluble biproducts are removed, see Appendix, Fig. A-2) and redissolved in a minimal amount of DMSO (20 mL) before precipitating a second time in 1 M acetic acid solution (150 mL). Vacuum filtration was performed followed by washing with ethanol. Dry yield was 1.05 g, 78 % (Figs. A-3 and A-4). Note: Once the **2** has been isolated, it has limited stability and will spontaneously form imine-cross-links, resulting in a dark brown insoluble solid (**3**) over the following weeks. ^1H NMR (500-MHz, DMSO- d_6) δ = 9.94 (s, 1H) and 8.98 (exchange, 2H); ^{13}C NMR (400-MHz, DMSO- d_6) δ = 185.93, 160.60, 95.68.

3. Analytical Techniques and Characterization

NMR spectroscopy was carried out with a 500-MHz Varian Inova or 400-MHz Varian Mercury spectrometer. DMSO- d_6 was used as the deuterated solvent for samples. All spectra were referenced to tetramethylsilane using residual ^1H or ^{13}C chemical shifts of the deuterated solvent.

FTIR spectra were collected using a Thermo Scientific Nicolet iS50R FTIR spectrometer equipped with a single reflection diamond attenuated total reflectance (ATR) module.

Powder X-ray diffraction (PXRD) data was collected using a PANalytical X'Pert Pro MPD, powered by a Philips PW3040/60 X-ray generator and fitted with an X'Celerator detector. Diffraction data is acquired by exposing powder samples to Cu K α 1 X-ray radiation, which has a characteristic wavelength of 1.5418 Å. Samples were mounted on zero background sample holders (glass slide) by dropping powders from a spatula and then leveling the sample. Data were collected using a 0.020° 2 θ step scan from 2 to 32° 2 θ with exposure time of 2 s per step.

Thermal gravimetric analysis (TGA) of 3 mg of sample contained in a Pt pan was performed using a TA Systems Q500 TGA instrument. Analysis was performed under nitrogen atmosphere (flow rate: 60 mL/min sample gas, 40 mL/min balance gas), with a heating rate of 10 °C/min from ambient temperature to 800 °C.

4. Results and Discussion

4.1 Reaction Mechanism

For NAS to be successful, both a good nucleophile and leaving group are required. Ammonia, with pK_a of approximately 34, satisfies as a good nucleophile, but bromine is only a moderate leaving group. Consideration of the NAS mechanism reveals that the rate-determining step is the nucleophilic attack on the aromatic ring (Fig. 3A). The resulting negative charge is resonance stabilized at the *ortho*- and *para*-positions of the ring, and further stabilized by the electron-withdrawing aldehyde groups at those positions. The success of this reaction can therefore largely be attributed to the presence and positions of the aldehyde groups.

Aside from the formation of **2**, it was initially hypothesized that, in addition to NAS of the bromines for amines, imines (Ar-CH=NH) could also form in place of the aldehydes. This would require nucleophilic attack by ammonia on the aldehyde carbon to form an aryl cyanohydrin, followed by dehydration to form the imine (Fig. 3B). However, no evidence of this process was observed experimentally, despite the reaction having been predicted to be exothermic and favored with a very negative Gibbs energy of reaction (Fig. A-1).

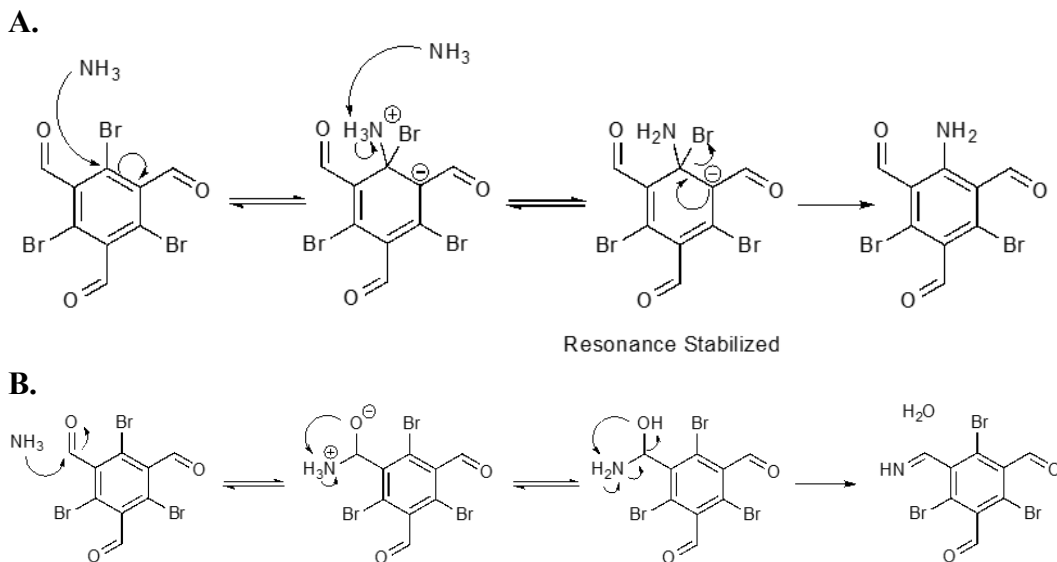


Fig. 3 Arrow-pushing reaction mechanism for NAS of ammonia with **1** (A), and the experimentally unobserved aldehyde amination (B)

4.2 Characterization of Products

The structure of **2** was confirmed by ^1H NMR with the appearance of an $-\text{NH}_2$ exchange peak at 8.98 ppm, which has a ratio of 1:1.72, compared to an expected ratio of 1:2 ratio between aldehyde and amine functionalities (Fig. 4). Furthermore, a slight shift in the aldehyde peak is seen from 10.10 ppm for **1** to 9.94 ppm for **2**, indicating the substitution of bromines for amines. NAS of the amines for bromines is also confirmed using ^{13}C NMR, which shows the disappearance of bromine-carbon resonances at 123.58 ppm, corresponding to **1**, and the appearance of an aryl carbon-nitrogen signal at 160.60 ppm (Fig. 5).

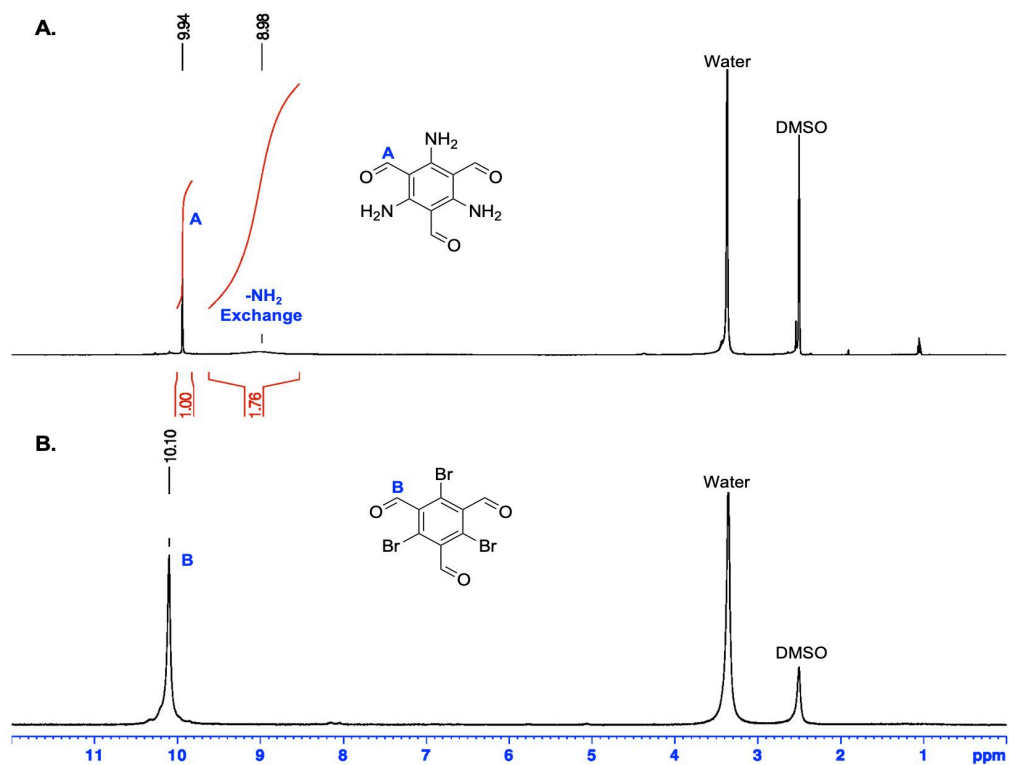


Fig. 4 ^1H NMR of 2 (A) and 1 (B) using 500-MHz spectrometer in $\text{DMSO-}d_6$

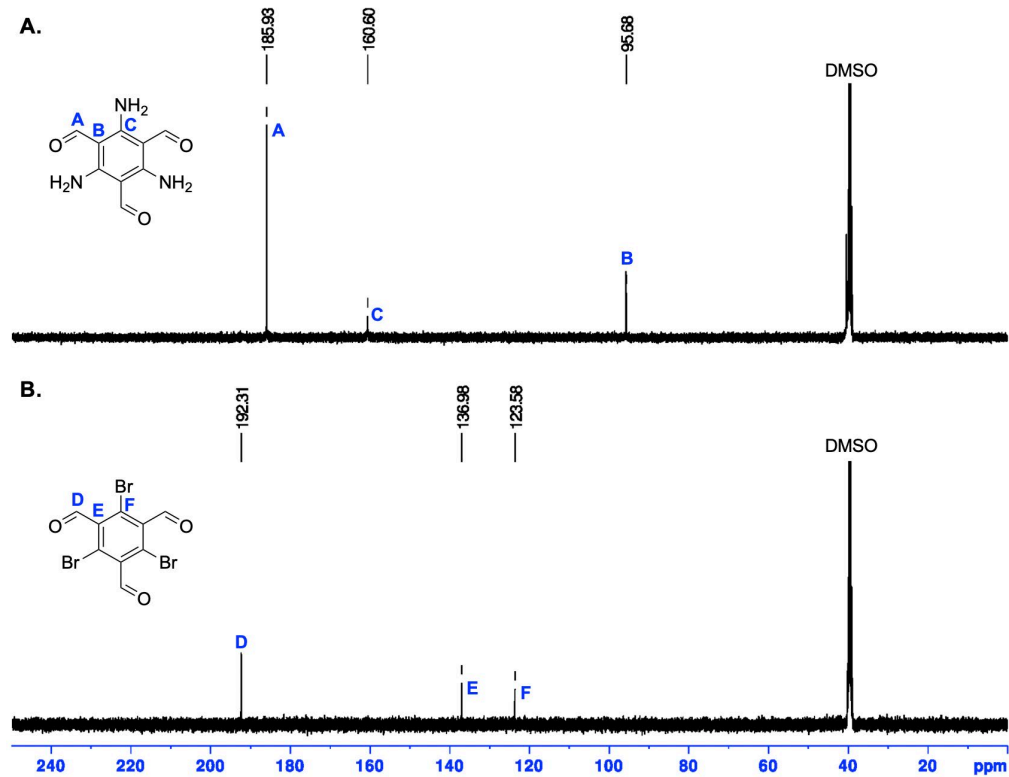


Fig. 5 ^{13}C NMR of 2 (A) and 1 (B) using 400-MHz spectrometer in $\text{DMSO-}d_6$

FTIR spectroscopy was used to analyze **2** and the insoluble dark brown solid **3**, which was spontaneously produced by **2** after sitting for several weeks (Fig. 6). For **2**, three peaks were observed within the amine range at 3360, 3312, and 3156 cm^{-1} , indicating the presence of the aryl amine. Additionally, the original aldehyde functionality seen in **1** is shifted from 1693 to 1660 cm^{-1} for **2**. Lastly, **3** has a significant reduction in the amine and aldehyde peaks compared to **2**, with the addition of a strong peak at 1650 cm^{-1} , indicating the presence of imine linkage that were not previously seen in the FTIR spectra **2**. Given the insolubility of **3** and the appearance of imine linkages, it is reasonable to conclude that the amines and aldehyde groups are reacting with each other to form an imine-based, cross-linked polymer.

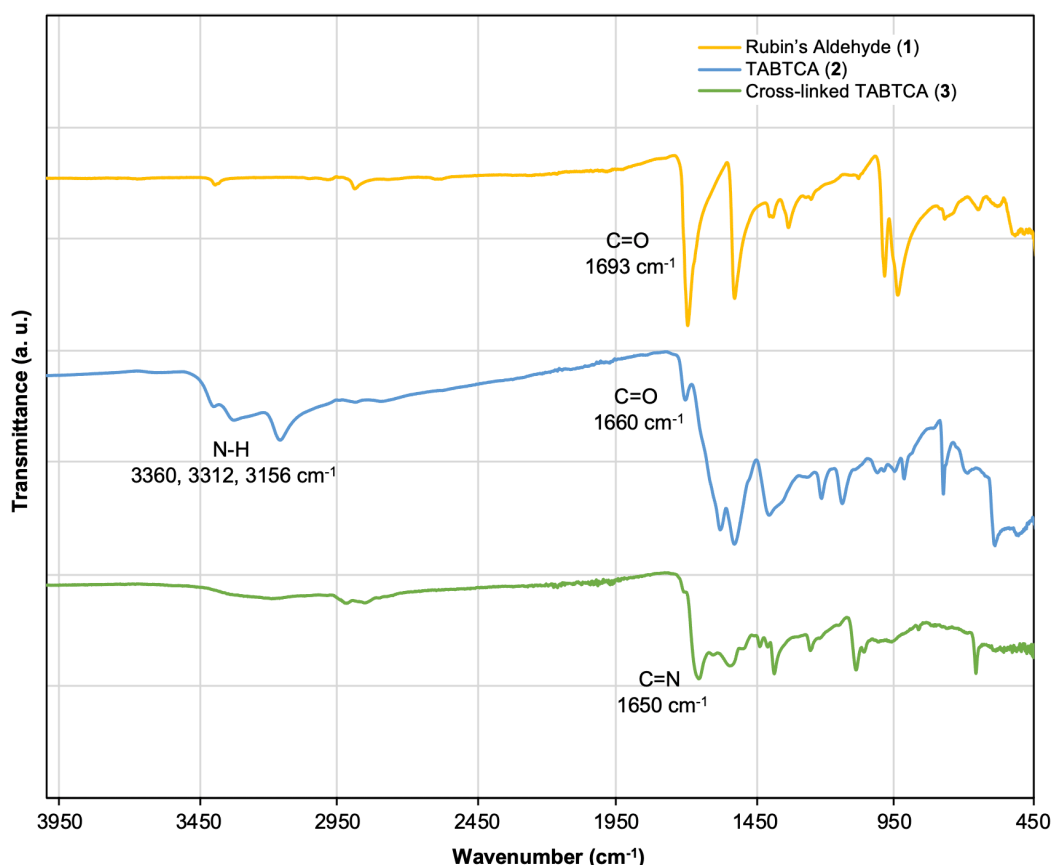


Fig. 6 FTIR spectra of Rubin's aldehyde (**1**), TABTCA (sample kl01-112-B) (**2**), and cross-linked TABTCA (sample kl01-91-solid) (**3**), with selected peaks and functional group assignment

Assignment of FTIR spectra peaks was performed after density functional theory (DFT) calculations were used to predict the IR frequencies of monomeric and cross-linked species. The initial structures of these species were constructed and approximated with molecular mechanics (MMFF94) using Avogadro.^{9,10} These structures were subjected to geometry optimization and frequency calculations at

the PBE0/6-311G** theoretical level using Gaussian 16.¹¹ The accuracy of various functionals were benchmarked in predicting the IR frequencies: B3LYP, HSEH1PBE, PBE, PBE0, and wB97XD. All predicted frequencies were scaled to account for approximation of the relativistic full configuration interaction wavefunction and anharmonicity of chemical bonds.^{12,13} Unpublished benchmarking studies indicate that the PBE0/6-311G** theoretical level accurately predicts the ATR-FTIR frequencies of similar aryl aldehyde molecules like terephthalaldehyde, aryl amine molecules like 1,3,5-tris(4-aminophenyl)benzene, and their expected imine products.

It is possible that **2** is spontaneously forming an organized imine-based 2D polymer over time; however, PXRD of **3** showed no diffraction signals, confirming that **3** has amorphous structure lacking any apparent crystallinity (Fig. 7).

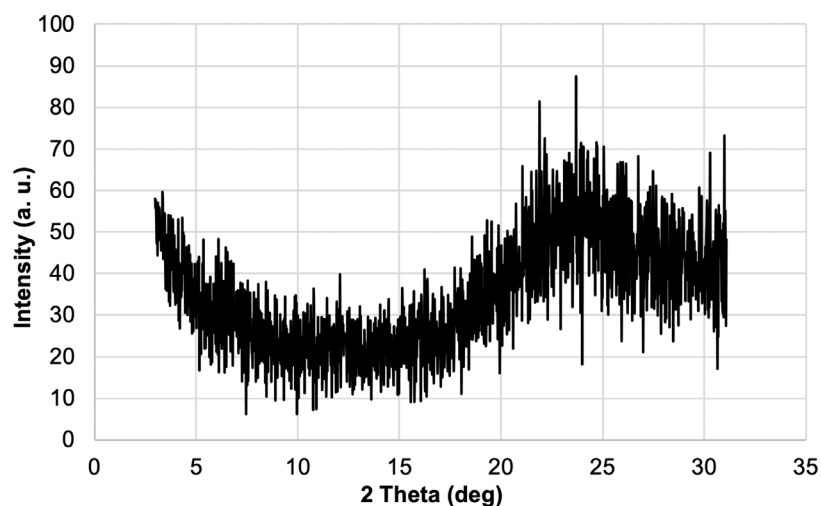


Fig. 7 PXRD of **3** (sample kl01-91-cross-linked) showing an absence of crystallinity

TGA indicates the onset of thermal decomposition begins at 220 °C for **2** (Fig. 8). Prior to 220 °C, less than 2.65% weight loss was observed, which can be attributed to removal of residual solvents. Between 225 and 400 °C the highest mass loss rate was observed, where 44% of the initial sample weight was lost. Beyond 400 °C, weight loss continued at a consisted rate until the maximum temperature of 800 °C is reached.

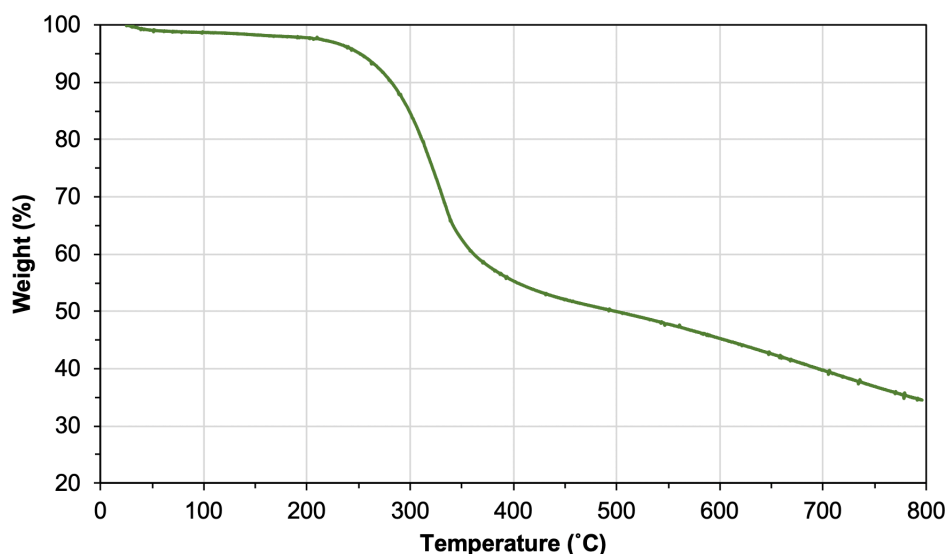


Fig. 8 TGA of **2**

4.3 Isolation and Stability of the Monomer

Post-reaction treatment of **2** is critical to extend its lifetime and stability. If **2** is simply precipitated in water and dried, it will quickly (within 3 h) form an amorphous cross-linked material, **3**, that is insoluble in all organic solvents except the strong organic acid trifluoroacetic acid, which is probably catalyzing hydrolysis of imine groups. NMR analysis of **3** does not reveal any useful information (Fig. A-6E). Analysis of the FTIR spectra of **3** suggests the possibility of imine linkages, as seen by a reduction in the intensities at the amine and aldehyde peaks, as well as some imine peaks at 1650 cm^{-1} (Fig. 6). In early attempts to isolate **2**, no precipitation was conducted, but rather the reaction solution was concentrated at $70\text{ }^{\circ}\text{C}$ under high vacuum. As the amount of DMSO was removed to less than 60% of its original volume, a cross-link gel was produced (Figs. A-5A and A-5B), which when dried has the same consistency and FTIR spectrum as **3** (Fig. A-6D). It is reasonable to conclude **3** is not generated while **2** is in a water suspension, since the presence of water disrupts and prevents the formation of imine linkage by forming hydrogen bonding networks. In an effort to avoid the spontaneous generation of **3**, while also being able to dry **2** to a suitable state for water-free reactions, formation of an ammonium salt through precipitation in acidic conditions was tested.

For comparison, three aliquots from the same reaction were precipitated into three separate solutions: 1) water, 2) 1 M HCl, and 3) 9.25 M HCl. For these experiments, 12.5 mL of the initial reaction solution was precipitated into 37.5 mL of each solution type and refrigerated for 18 h, then the precipitate was collected using vacuum filtration, washed with ethanol, dried, and finally analyzed via ^{13}C NMR

(Fig. 9). The compound precipitated in only water had no trace of aryl-halide resonances, indicating complete success in converting **1** to **2**; however, the isolated compound rapidly formed the cross-linked material **3** in about 3 h. The compound precipitated in 1 M HCl was relatively stable but had signals indicating some formation of aryl-halide bonds instead of aryl-amine bonds. Precipitation in the 9.25 M HCl solution gave complete reversal of the NAS process, showing only the presence of aryl-halide bonds.

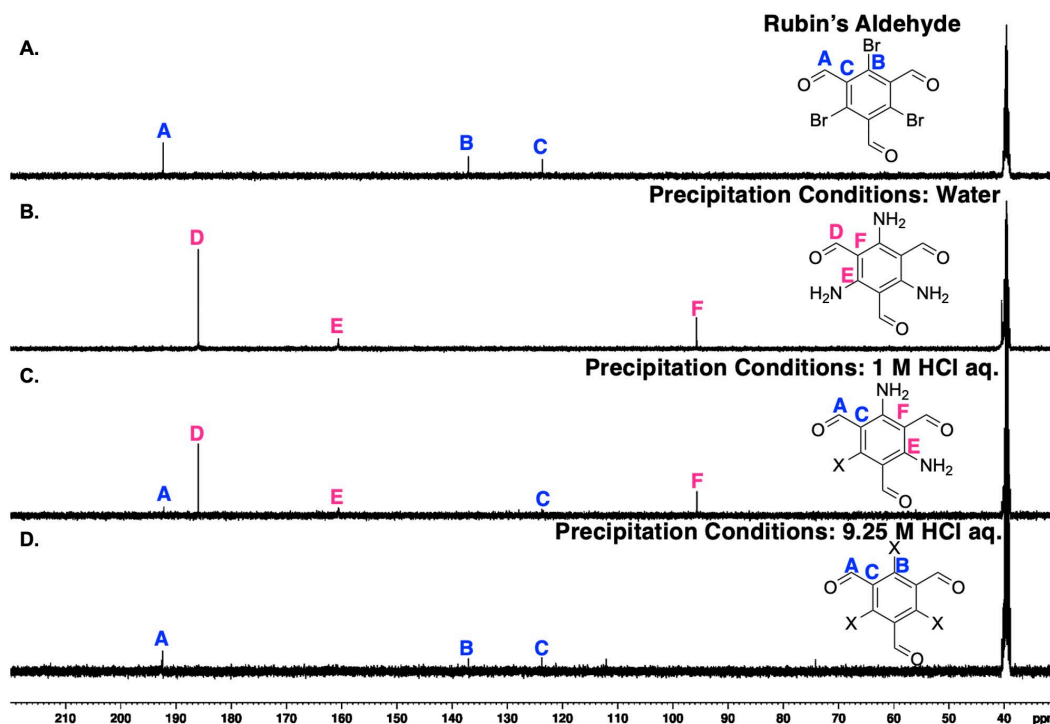


Fig. 9 ^{13}C NMR collected with a 500-MHz spectrometer of **1** (A), **2** prepared through precipitation in water (B), 1 M HCl (C), and 9.25 M HCl (D) in $\text{DMSO-}d_6$

A final solution of 1 M acetic acid solution was tested to compare the effects of a weak acid on **2**. This solution has the desired effect, in that the resulting product was stabilized, any residual ammonia was removed, and there is no evidence of undesired side reactions or decomposition (Fig. 10). Using this method, conversion of **2** to **3** is slowed from 3 h, when precipitated in water, to over 3 weeks.

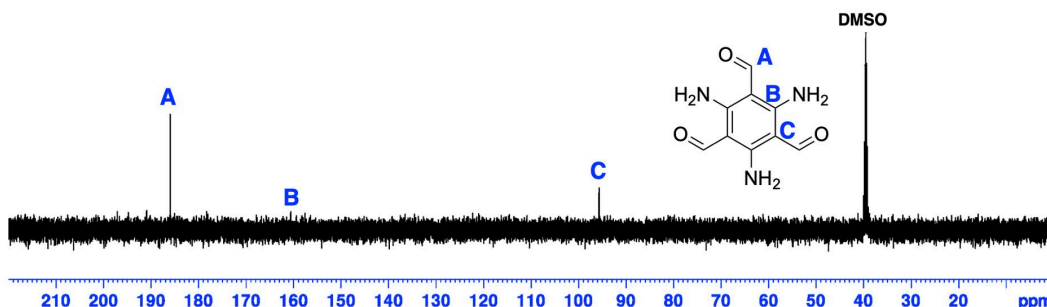


Fig. 10 ^{13}C NMR collected with a 500-MHz spectrometer of **2** prepared through precipitation in 1 M acetic acid, in $\text{DMSO-}d_6$

In all types of acidic precipitation conditions, it was expected an ammonium salt was formed that resulted in the increased stability of **2**, preventing the spontaneous formation of **3**. However, ^1H NMR analysis revealed no difference between the presumably protonated (labeled as **4**) and unprotonated forms of **2** (Fig. A-7). It was expected that there would be an increase between aldehyde and amine integration values from approximately 1:2 to 1:3, but this was not observed.

To elucidate the state of the monomer, molecular mechanics were used to predict the IR absorbances of the neutral compound **2** (Table A-1) and the protonated ammonium compound **4** (Table A-4). Two samples of the monomer were compared to these DFT-derived IR vibrations. One sample (labeled kl01-91-monomer) was precipitated in water, which allowed for rapid reaction of **2** into **3**, presumably because the amines are neutral and not in the relatively unreactive, protonated state. Comparisons of the DFT-derived IR vibrations from **4** and **2** to experimental data on the water precipitated compound (kl01-91-monomer) are given in Tables A-3 and A-6, respectively. A second sample (labeled as kl01-112-B) was purified through precipitation in 1 M HCl, generating a stable compound that did not immediately cross-link. The process of precipitating in an acid solution is thought to eliminate any residual ammonia from the resulting product and protonate the amine, creating a stable ammonium salt complex. Comparisons of the DFT-derived IR vibrations from **4** and **2** to experimental data on the HCl-precipitated compound (kl01-112-B) are given in Tables A-1.2 and A- 2.2, respectively. Interestingly, both products match the DFT-derived IR vibrations for the protonated species better than the neutral species. This conclusion was made from the analysis of the peaks, where more experimental peaks matched high-intensity computational peaks (high-intensity peaks are determined to be any peak with a value >0.00), and consistently had errors of less than 1%.

5. Conclusions and Future Directions

Here we report a simple, one-step method for producing 2,4,6-triaminobenzene-1,3,5-tricarboxylaldehyde, **2**, from Rubin's aldehyde, **1**, using anhydrous ammonia in a DMSO solution. The resulting product has limited solubility and stability, making further purification difficult, but the process is efficient and has good yield. Using 1 M acetic acid solution for precipitation, the amine residue appears to be stabilized; however, the final state of the monomer is unclear because there is no change in NMR between protonated and unprotonated forms. DFT-derived FTIR vibrational modes support that **2** is closer to a protonated form than the unprotonated structure. In future work, **2** will be polymerized into a variety of 2D COFs, either by itself or in the presence of comonomers. Additionally, this compound may prove useful as a precursor to other high-value, nitrogen-rich chemicals such as pharmaceuticals and energetic compounds.

6. References

1. McLeod DC, Lachmayr KK, Lambeth RH, Switek A, Murphy A, Pesce-Rodriguez RA, Lustig SR. Synthesis of a novel hexa-functional monomer for 2D polymers: 2,4,6-tris((diphenylmethylene) amino)benzene-1,3,5-tricarbaldehyde. DEVCOM Army Research Laboratory (US); Forthcoming 2023.
2. Aubin Y, Fischmeister C, Thomas CM, Renaud JL. Direct amination of aryl halides with ammonia. *Chem Soc Rev*. 2010;39:4130–4145.
3. Werner EA. LXXX–I.—The preparation of ethylamine and of diethylamine. *J Chem Soc Trans*. 1918;113:899–902.
4. Bordwell FG, Algrim DJ. Acidities of anilines in dimethyl sulfoxide solution. *J Am Chem Soc*. 1988;110:2964–2968.
5. Engineering ToolBox. Ammonia-vapour pressure at gas-liquid equilibrium. 2003 [accessed 2021 Aug 21]. https://www.engineeringtoolbox.com/ammonia-pressure-temperature-d_361.html.
6. Gaylord Chemical Company. Dimethyl sulfoxide solubility data. 2014 [accessed 2021 Aug 21]. <https://gaylordchemical.com/content/uploads/2020/08/GC-Literature-102B-ENG-Low.pdf>.
7. Short I, Sahgal A, Hayduk W. Solubility of ammonia and hydrogen sulfide in several polar solvents. *J Chem Eng Data*. 1983;28:63–66.
8. Holst C, Schollmeyer D, Meier H. An efficient synthesis of Rubin's aldehyde and its precursor 1,3,5-tribromo-2,4,6-tris(dichloromethyl)benzene. *Z Naturforsch*. 2011;66b:935–938.
9. Halgren TA. Merck molecular force field. I. Basis, form, scope, parameterization, and performance of MMFF94. *J Comput Chem*. 1996;17:490–519.
10. Hanwell MD, Curtis DE, Lonie DC, Vandermeersch T, Zurek E, Hutchison GR. Avogadro: an advanced semantic chemical editor, visualization, and analysis platform. *J Cheminformatics*. 2012;4:17.
11. Frisch MJ, Trucks GW, Schlegel HB, Scuseria GE, Robb MA, Cheeseman JR, Scalmani G, Barone V, Petersson GA, Nakatsuji H, et al. Gaussian 16 Rev. C.01. Gaussian, Inc. 2016 [accessed 2022 May 27].

12. National Institute of Standards and Technology. Precomputed vibrational scaling factors. National Institute of Standards and Technology; 2013 [accessed 2022 May 27]. <https://cccbdb.nist.gov/vibscalejust.asp>.
13. National Institute of Standards and Technology. Vibrational scaling factors. National Institute of Standards and Technology. 2013 [accessed 2022 May 27]. <https://cccbdb.nist.gov/vibnotes.asp>.

Appendix. Supplementary Information

Figure A-1 shows molecular mechanics modeling of Gibbs energy of reaction. Figures A-2 through A-6 include additional ^1H nuclear magnetic resonance (NMR) spectra. Figures A-3 through A-5 include photographs of various reaction intermediates and isolated products.

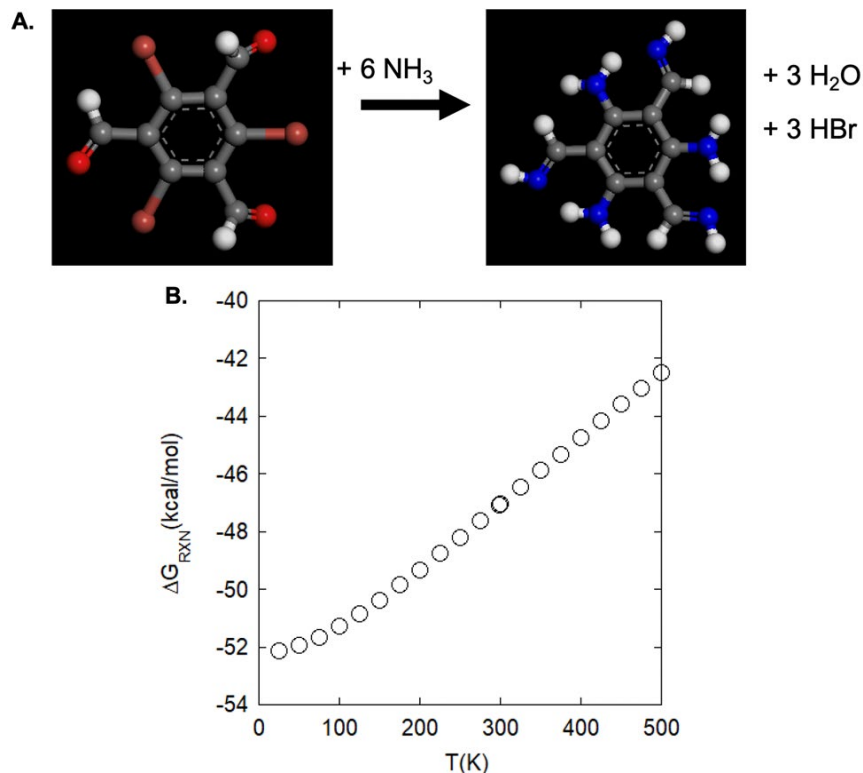


Fig. A-1 Reaction scheme showing the conversion of **1** to 2,4,6-tris(iminomethyl)benzene-1,3,5-triamine, through the addition of six ammonia molecules and removal of three water and three HBr molecules (**A**). Reaction is predicted, via molecular mechanics, to be exothermic and favored with a very negative Gibbs energy of reaction (**B**).

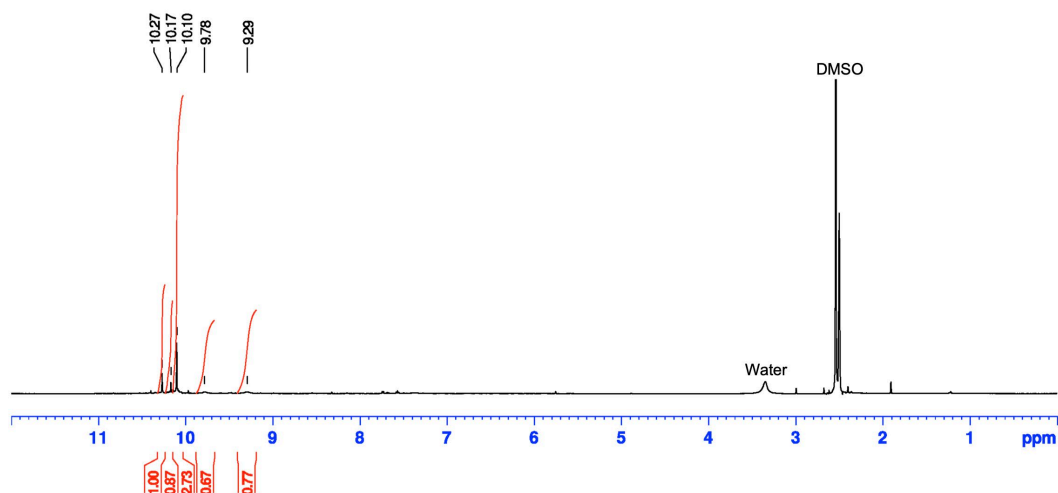


Fig. A-2 ^1H NMR of products removed from dichloromethane (DCM) washing of crude product 2, collected on a 500-MHz spectrometer using dimethyl sulfoxide (DMSO)- d_6



Fig. A-3 Compound 2 collected in at the bottom of a fritted funnel

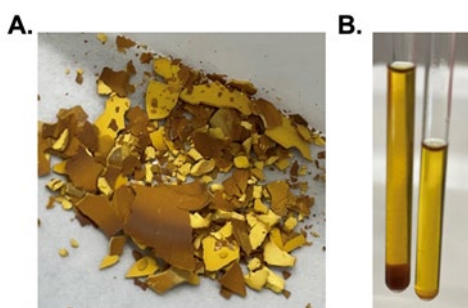


Fig. A-4 Photographs of a mixture of 2 and 3. A neat reaction solution producing 2 was allowed to dry under air for 3 days, resulting in a layer effect of 2 on the bottom surface sandwiched between glass and a top layer of 3 that was exposed to air (A). NMR tubes contain a DMSO solution of a 2 and 3 mixture, where 2 is soluble in DMSO , producing a yellow solution, and 3 is insoluble, forming a brown solid at the bottom of the left tube (B).

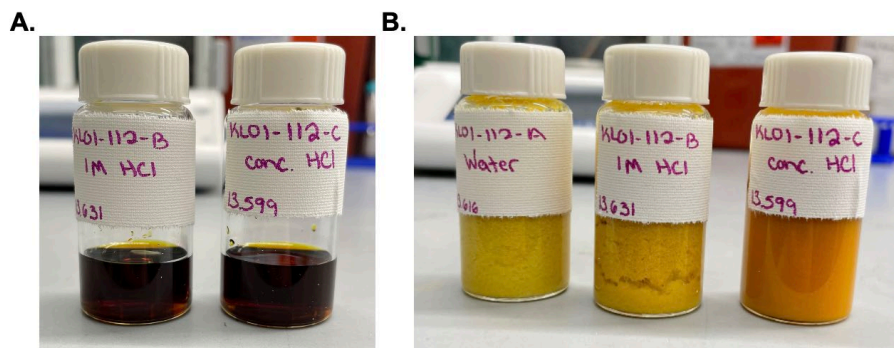


Fig. A-5 Initial crude reaction solution of compound 2 (A), which was the precipitated in water, 1 M HCl, and 9.25 M HCl (B) to analyze amine-salt formation and stabilization of 2

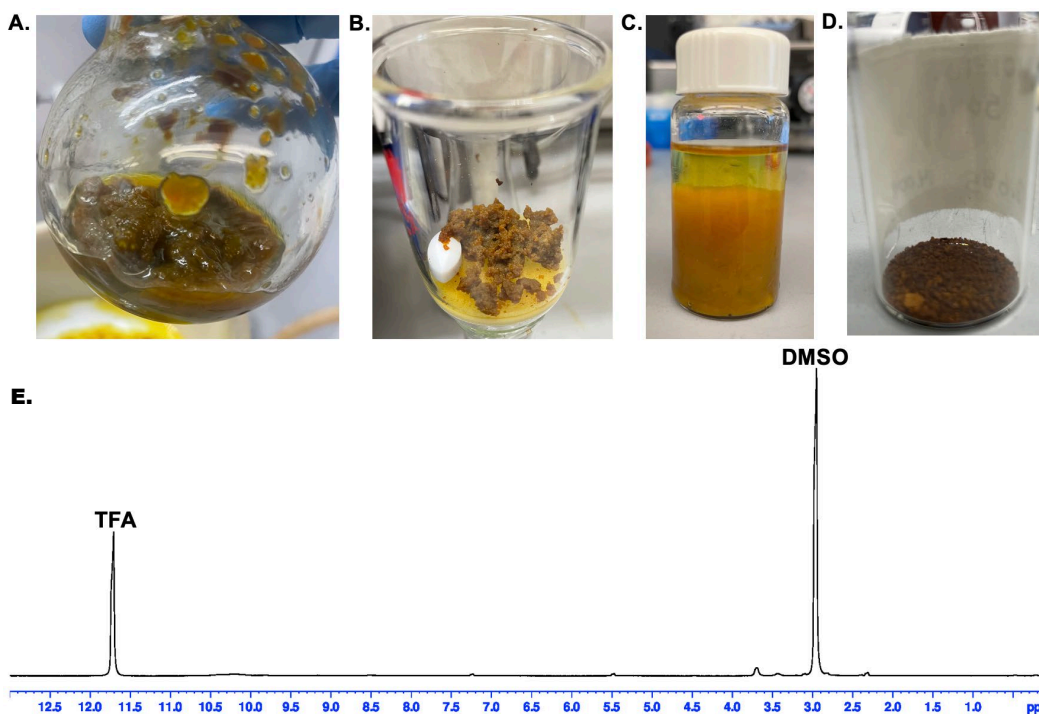


Fig. A-6 Concentration of the crude reaction solution containing 2 in DMSO to 70 °C under high vacuum results in the formation of a gel-like substance (A). This gel was isolated and washed with fresh DMSO (B) and re-solubilization in DMSO was attempted (C) to recover unreacted 2, with poor results. Drying under high vacuum to remove DMSO resulted in 3 as a powdered substance (D) that appears soluble in trifluoroacetic acid. The powder has no proton resonances (E), but has Fourier transform infrared (FTIR) spectra consistent with other 3 that were formed without prior gelation.

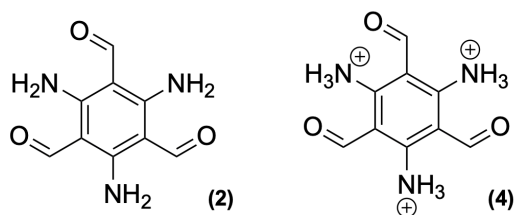


Fig. A-7 Comparison of neutral (2) and charged structures (4)

Tables A-1 through A-6 are comparisons of calculated IR vibrational modes derived from density functional theory (DFT). Table A-1 is the protonated compound, **4**, and Table A-4 is the unprotonated compound **2**. For these tables, the frequencies (Freq.) (column 1) and intensities (Inten.) (column 3) are generated using DFT calculations, and the scaled calculations are the product of the calculated frequencies (column 1) multiplied by a scaling factor of 0.9909.^{1,2} Selected peaks include an animation description, generated by the author, to describe the functional groups active within each vibrational mode.

Table A-1 DFT-derived frequencies, scale frequencies, intensities, and selected animation descriptions for 4

Freq. (cm ⁻¹)	Scaled (cm ⁻¹)	Inten. (km/mol)	Description
3345.05	3314.61	46.57	Amine proton out of plane bending
3344.46	3314.03	0.00	...
3344.41	3313.98	0.12	Amine proton out of plane bending
3290.06	3260.12	0.00	...
3287.08	3257.17	30.94	Amine proton out of plane stretching
3287.04	3257.13	30.93	Amine proton out of plane stretching
2971.23	2944.19	0.51	Carbonyl proton bending
2971.18	2944.14	0.50	...
2970.87	2943.84	0.01	...
2319.88	2298.77	100.00	...
2319.64	2298.53	100.00	...
2294.47	2273.59	0.00	...
1700.69	1685.21	8.25	Amine and carbonyl
1700.63	1685.15	8.26	Amine and carbonyl
1700.21	1684.74	0.07	Amine and carbonyl
1608.98	1594.34	0.16	...

¹ Frisch MJ, Trucks GW, Schlegel HB, Scuseria GE, Robb MA, Cheeseman JR, Scalmani G, Barone V, Petersson GA, Nakatsuji H, et al. Gaussian 16 Rev. C.01. Gaussian, Inc. 2016 [accessed 2022 May 27].

² National Institute of Standards and Technology. Precomputed vibrational scaling factors. National Institute of Standards and Technology; 2013 [accessed 2022 May 27]. <https://cccbdb.nist.gov/vibscalejust.asp>.

Table A-1 DFT-derived frequencies, scale frequencies, intensities, and selected animation descriptions for 4 (continued)

Freq. (cm ⁻¹)	Scaled (cm ⁻¹)	Inten. (km/mol)	Description
1608.64	1594.00	0.01	...
1606.81	1592.19	15.18	Amine proton stretching
1599.59	1585.03	7.37	Amine proton stretching and benzene
1599.45	1584.90	7.29	...
1567.94	1553.67	0.00	...
1538.69	1524.69	23.54	Whole molecule
1538.63	1524.63	23.57	...
1481.23	1467.75	0.08	...
1476.95	1463.51	31.90	Whole molecule
1476.64	1463.20	31.99	...
1387.54	1374.91	0.00	Carbonyl protons and benzene
1378.68	1366.13	2.00	Protons and benzene
1378.43	1365.89	2.01	...
1341.38	1329.17	4.02	...
1341.14	1328.94	4.00	...
1301.16	1289.32	0.00	Whole molecule
1208.19	1197.20	0.00	Benzene stretching
1199.07	1188.16	0.00	Whole molecule
1118.99	1108.81	0.00	...
1101.64	1091.62	0.00	...
1101.57	1091.55	0.00	...
1093.65	1083.70	1.46	...
1090.12	1080.20	2.06	...
1089.93	1080.01	2.04	Amine and benzene
1003.06	993.93	5.90	...
1003.02	993.89	5.90	Benzene ring distortion
970.109	961.28	0.00	Carbonyl proton and benzene
970.09	961.26	0.00	Carbonyl proton and benzene
964.224	955.45	0.41	Carbonyl proton bending and some amine bending
838.951	831.32	18.80	...
838.799	831.17	18.79	...
797.68	790.42	0.00	Whole molecule
738.471	731.75	0.05	Benzene and amine bending
591.295	585.91	0.06	...
591.215	585.83	0.01	...
590.841	585.46	2.99	...
590.782	585.41	3.05	Benzene and carbonyl bending
548.527	543.54	0.00	...
541.802	536.87	0.00	...
416.278	412.49	9.71	...
415.994	412.21	9.65	...
415.55	411.77	0.01	...
415.084	411.31	0.05	...
411.295	407.55	0.11	...
385.597	382.09	0.00	...
372.607	369.22	2.03	...
372.529	369.14	2.04	...

Table A-1 (U) DFT-derived frequencies, scale frequencies, intensities, and selected animation descriptions for 4 (continued)

Freq. (cm⁻¹)	Scaled (cm⁻¹)	Inten. (km/mol)	Description
371.254	367.88	0.00	...
345.103	341.96	0.00	...
345.056	341.92	0.00	...
245.101	242.87	7.82	...
230.866	228.77	1.48	...
230.759	228.66	1.50	...
172.694	171.12	0.00	...
172.367	170.80	0.00	...
150.534	149.16	0.35	...
90.5814	89.76	2.92	...
70.8426	70.20	0.00	...
70.649	70.01	0.00	...

Table A-2 Comparison of select computational DFT data from 4 to experimental data on compound kl01-112-B. Intensities are in percent transmittance for experimental data.

Calculated FTIR vibrational modes			Experimental data from kl01-112-B			Percent error	
Freq. (cm⁻¹)	Scaled (cm⁻¹)	Inten. (km/mol)	Freq. (cm⁻¹)	Inten. (%)	Peak shape	Freq. (%)	Scaled (%)
3345.05	3314.61	46.57	3396.568	74.927	Broad	1.54	2.47
3344.46	3314.03	0.00
3344.41	3313.98	0.12	3318.464	68.9801	Broad	-0.78	0.13
3290.06	3260.12	0.00
3287.08	3257.17	30.94	3154.06	60.219	Broad	-4.05	-3.17
3287.04	3257.13	30.93
2971.23	2944.19	0.51
2971.18	2944.14	0.50
2970.87	2943.84	0.01
2319.88	2298.77	100.00
2319.64	2298.53	100.00
2294.47	2273.59	0.00
1700.69	1685.21	8.25	1699.972	78.046	Sharp	-0.04	0.88
1700.63	1685.15	8.26	1645.732	62.027	Shoulder	-3.23	-2.34
1700.21	1684.74	0.07	1611.742	40.38	Shoulder	-5.20	-4.33
1608.98	1594.34	0.16
1608.64	1594.00	0.01
1606.81	1592.19	15.18	1592.699	30.25	Shoulder	-0.88	0.03
1599.59	1585.03	7.37	1574.86	19.995	Broad	-1.55	-0.64
1599.45	1584.90	7.29
1567.94	1553.67	0.00
1538.69	1524.69	23.54	1523.273	13.701	Broad	-1.00	-0.09
1538.63	1524.63	23.57
1481.23	1467.75	0.08
1476.95	1463.51	31.90	1474.578	42.039	Shoulder	-0.16	0.76

Table A-2 Comparison of select computational DFT data from 4 to experimental data on compound kl01-112-B. Intensities are in percent transmittance for experimental data. (continued)

Calculated FTIR vibrational modes			Experimental data from kl01-112-B			Percent error	
Freq. (cm ⁻¹)	Scaled (cm ⁻¹)	Inten. (km/mol)	Freq. (cm ⁻¹)	Inten. (%)	Peak shape	Freq. (%)	Scaled (%)
1476.64	1463.20	31.99
1387.54	1374.91	0.00	1397.92	26.561	Broad	0.75	1.67
1378.68	1366.13	2.00	1350.913	32.959	Shoulder – broad	–2.01	–1.11
1378.43	1365.89	2.01
1341.38	1329.17	4.02
1341.14	1328.94	4.00
1301.16	1289.32	0.00	1260.756	43.446	Small broad	–3.11	–2.22
1208.19	1197.20	0.00	1212.061	33.959	Sharp	0.32	1.24
1199.07	1188.16	0.00	1137.814	31.5581	Sharp	–5.11	–4.24
1118.99	1108.81	0.00
1101.64	1091.62	0.00
1101.57	1091.55	0.00
1093.65	1083.70	1.46
1090.12	1080.20	2.06
1089.93	1080.01	2.04	1078.031	48.003	Broad	–1.09	–0.18
1003.06	993.93	5.90
1003.02	993.89	5.90	1009.087	45.54	Small broad	0.60	1.53
970.109	961.28	0.00	986.9091	46.244	Small	1.73	2.67
970.09	961.26	0.00	949.7855	45.905	Small	–2.09	–1.19
964.224	955.45	0.41	915.313	42.6855	Small sharp	–5.07	–4.20
838.951	831.32	18.80
838.799	831.17	18.79
797.68	790.42	0.00	774.292	36.11	Sharp	–2.93	–2.04
738.471	731.75	0.05	686.54	45.191	Broad	–7.03	–6.18
591.295	585.91	0.06
591.215	585.83	0.01
590.841	585.46	2.99
590.782	585.41	3.05	588.67	12.99	Sharp – tail to right	–0.36	0.56

Table A-3 Comparison of select computational DFT data from 4 to experimental data on compound kl01-91-monomer. Intensities are in percent transmittance for experimental data.

Calculated FTIR vibrational modes			Experimental data from kl01-91			Percent error	
Freq. (cm ⁻¹)	Scaled (cm ⁻¹)	Inten. (km/mol)	Freq. (cm ⁻¹)	Inten. (%)	Peak shape	Freq. (%)	Scaled (%)
3345.05	3314.61	46.57	3401.148	82.81	Sharp	1.68	2.61
3344.46	3314.03	0.00
3344.41	3313.98	0.12	3325.696	81.18	Sharp – right tail	–0.56	0.35
3290.06	3260.12	0.00
3287.08	3257.17	30.94	3158.881	74.85	Sharp	–3.90	–3.02
3287.04	3257.13	30.93
2971.23	2944.19	0.51	2810.546	91.6	Small broad	–5.41	–4.54
2971.18	2944.14	0.50
2970.87	2943.84	0.01
2319.88	2298.77	100.00
2319.64	2298.53	100.00
2294.47	2273.59	0.00
1700.69	1685.21	8.25
1700.63	1685.15	8.26	1654.65	89.166	Shoulder	–2.70	–1.81
1700.21	1684.74	0.07	1610.055	61.113	Shoulder	–5.30	–4.43
1608.98	1594.34	0.16
1608.64	1594.00	0.01
1606.81	1592.19	15.18	1597.038	56.115 7	Shoulder	–0.61	0.30
1599.59	1585.03	7.37	1579.681	41.747	Sharp	–1.24	–0.34
1599.45	1584.90	7.29
1567.94	1553.67	0.00
1538.69	1524.69	23.54	1530.746	44.216	Sharp	–0.52	0.40
1538.63	1524.63	23.57
1481.23	1467.75	0.08
1476.95	1463.51	31.90	1474.096	74.43	Shoulder	–0.19	0.72
1476.64	1463.20	31.99
1387.54	1374.91	0.00	1405.634	53.152	Broad	1.30	2.23
1378.68	1366.13	2.00
1378.43	1365.89	2.01
1341.38	1329.17	4.02
1341.14	1328.94	4.00
1301.16	1289.32	0.00	1259.792	75.27	Small	–3.18	–2.29
1208.19	1197.20	0.00	1214.472	63.26	Sharp	0.52	1.44
1199.07	1188.16	0.00	1139.743	56.81	Sharp – right tail	–4.95	–4.07
1118.99	1108.81	0.00	1096.833	73.46	Shoulder	–1.98	–1.08
1101.64	1091.62	0.00
1101.57	1091.55	0.00
1093.65	1083.70	1.46

Table A-3 Comparison of select computational DFT data from 4 to experimental data on compound kl01-91-monomer. Intensities are in percent transmittance for experimental data. (continued)

Calculated FTIR vibrational modes			Experimental data from kl01-91			Percent error	
Freq. (cm ⁻¹)	Scaled (cm ⁻¹)	Inten. (km/mol)	Freq. (cm ⁻¹)	Inten. (%)	Peak shape	Freq. (%)	Scaled (%)
1090.12	1080.20	2.06
1089.93	1080.01	2.04
1003.06	993.93	5.90	1021.863	76.9	Small Sharp	1.87	2.81
1003.02	993.89	5.90
970.109	961.28	0.00
970.09	961.26	0.00
964.224	955.45	0.41	916.76	68.52	Sharp	-4.92	10.28
838.951	831.32	18.80
838.799	831.17	18.79
797.68	790.42	0.00	774.7743	55.99	Sharp	-2.87	-1.98
738.471	731.75	0.05	693.0542	76.3	Broad	-6.15	-5.29
591.295	585.91	0.06
591.215	585.83	0.01
590.841	585.46	2.99
590.782	585.41	3.05	590.8438	31.199	Sharp – right tail	0.01	0.93

Table A-4 DFT-derived frequencies, scale frequencies, intensities, and selected animation descriptions for 2

Freq. (cm⁻¹)	Scaled (cm⁻¹)	Inten. (km/mol)	Description
3603.7	3570.9	4.4	...
3603.4	3570.6	6.7	...
3601.8	3569.0	6.0	...
3182.5	3153.6	34.1	Amine proton rocking
3180.8	3151.8	31.1	Amine proton rocking
3175.7	3146.8	3.7	Amine proton rocking
2824.1	2798.4	18.6	...
2823.6	2797.9	13.3	...
2822.2	2796.5	7.8	...
1648.5	1633.4	0.0	...
1638.0	1623.0	33.3	Whole molecule rocking
1637.8	1622.9	33.8	Carbonyl bending and amine protons
1595.1	1580.6	1.3	...
1590.8	1576.3	100.0	Benzene and amine
1590.5	1576.0	98.8	Amine protons and benzene
1529.0	1515.1	6.4	...
1528.4	1514.5	6.1	...
1444.9	1431.8	0.0	...
1428.0	1415.0	0.7	...
1427.2	1414.2	0.9	Whole molecule
1414.7	1401.9	0.0	Whole molecule
1393.6	1381.0	22.3	...
1393.2	1380.5	22.8	Whole molecule
1345.4	1333.1	0.0	Benzene ring
1287.1	1275.4	0.0	...
1208.1	1197.1	2.4	Whole molecule
1207.8	1196.8	2.3	...
1181.0	1170.2	0.0	Whole molecule
1147.9	1137.5	3.8	...
1147.5	1137.0	3.8	...
943.4	934.8	0.0	Carbonyl proton bending
940.5	932.0	0.0	...
937.0	928.5	0.0	...
907.7	899.5	1.2	Whole molecule
907.4	899.2	1.2	...
804.2	796.9	0.0	...
790.1	782.9	11.0	...
789.8	782.6	2.9	...
788.3	781.1	0.5	Amine proton
759.7	752.7	0.0	...
678.6	672.4	0.0	...
677.8	671.6	0.0	...
609.5	604.0	0.0	...
595.8	590.4	6.1	Whole molecule
595.4	590.0	6.0	...
563.7	558.6	0.0	...

Table A-5 Comparison of select computational DFT data from 2 to experimental data on compound kl01-122-B. Intensities are in percent transmittance for experimental data.

Calculated FTIR vibrational modes			Experimental data from kl01-112-B			Percent error	
Freq. (cm ⁻¹)	Scaled (cm ⁻¹)	Inten. (km/mol)	Freq. (cm ⁻¹)	Inten. (%)	Peak shape	Freq. (%)	Scaled (%)
3603.7	3570.9	4.4	3396.568	74.927	Broad	-5.75	-4.88
3603.4	3570.6	6.7	3318.464	68.9801	Broad	-7.91	-7.06
3601.8	3569.0	6.0	3154.06	60.219	Broad	-12.43	-11.63
3182.5	3153.6	34.1
3180.8	3151.8	31.1
3175.7	3146.8	3.7
2824.1	2798.4	18.6
2823.6	2797.9	13.3
2822.2	2796.5	7.8
1648.5	1633.4	0.0
1638.0	1623.0	33.3	1699.972	78.046	Sharp	3.79	4.74
1637.8	1622.9	33.8	1645.732	62.027	Shoulder	0.49	1.41
1595.1	1580.6	1.3	1611.742	40.38	Shoulder	1.04	1.97
1590.8	1576.3	100.0	1592.699	30.25	Shoulder	0.12	1.04
1590.5	1576.0	98.8	1574.86	19.995	Broad	-0.98	-0.07
1529.0	1515.1	6.4
1528.4	1514.5	6.1	1523.273	13.701	Broad	-0.34	0.58
1444.9	1431.8	0.0	1474.578	42.039	Shoulder	2.05	2.99
1428.0	1415.0	0.7
1427.2	1414.2	0.9
1414.7	1401.9	0.0	1397.92	26.561	Broad	-1.19	-0.28
1393.6	1381.0	22.3
1393.2	1380.5	22.8	1350.913	32.959	Shoulder – broad	-3.03	-2.14
1345.4	1333.1	0.0	1260.756	43.446	Small broad	-6.29	-5.43
1287.1	1275.4	0.0
1208.1	1197.1	2.4	1212.061	33.959	Sharp	0.32	1.25
1207.8	1196.8	2.3
1181.0	1170.2	0.0	1137.814	31.5581	Sharp	-3.65	-2.77
1147.9	1137.5	3.8
1147.5	1137.0	3.8
943.4	934.8	0.0	949.7855	45.905	Small	0.68	1.60
940.5	932.0	0.0
937.0	928.5	0.0
907.7	899.5	1.2	915.313	42.6855	Small sharp	0.84	1.76
907.4	899.2	1.2
804.2	796.9	0.0
790.1	782.9	11.0
789.8	782.6	2.9
788.3	781.1	0.5	774.292	36.11	Sharp	-1.78	-0.88
759.7	752.7	0.0
678.6	672.4	0.0	686.54	45.191	Broad	1.18	2.10
677.8	671.6	0.0
609.5	604.0	0.0
595.8	590.4	6.1	588.67	12.99	Sharp – tail to right	-1.20	-0.29
595.4	590.0	6.0
563.7	558.6	0.0

Table A-6 Comparison of select computational DFT data from 2 to experimental data on compound kl01-91-monomer. Intensities are in percent transmittance for experimental data.

Calculated FTIR vibrational modes			Experimental data from kl01-91			Percent error	
Freq. (cm ⁻¹)	Scaled (cm ⁻¹)	Inten. (km/mol)	Freq. (cm ⁻¹)	Inten. (%)	Peak shape	Freq. (%)	Scaled (%)
3603.7	3570.9	4.4	3401.148	82.81	Sharp	-5.62	-4.75
3603.4	3570.6	6.7	3325.696	81.18	Sharp – right tail	-7.71	-6.86
3601.8	3569.0	6.0	3158.881	74.85	Sharp	-12.30	-11.49
3182.5	3153.6	34.1
3180.8	3151.8	31.1
3175.7	3146.8	3.7	2810.546	91.6	Small broad	-11.50	-10.69
2824.1	2798.4	18.6
2823.6	2797.9	13.3
2822.2	2796.5	7.8
1648.5	1633.4	0.0
1638.0	1623.0	33.3
1637.8	1622.9	33.8	1654.65	89.166	Shoulder	1.03	1.96
1595.1	1580.6	1.3	1610.055	61.113	Shoulder	0.94	1.87
1590.8	1576.3	100.0	1597.038	56.1157	Shoulder	0.39	1.32
1590.5	1576.0	98.8	1579.681	41.747	Sharp	-0.68	0.23
1529.0	1515.1	6.4
1528.4	1514.5	6.1	1530.746	44.216	Sharp	0.15	1.07
1444.9	1431.8	0.0	1474.096	74.43	Shoulder	2.02	2.95
1428.0	1415.0	0.7
1427.2	1414.2	0.9	1405.634	53.152	Broad	-1.51	-0.61
1414.7	1401.9	0.0
1393.6	1381.0	22.3
1393.2	1380.5	22.8
1345.4	1333.1	0.0	1259.792	75.27	Small	-6.36	-5.50
1287.1	1275.4	0.0
1208.1	1197.1	2.4	1214.472	63.26	Sharp	0.52	1.45
1207.8	1196.8	2.3
1181.0	1170.2	0.0	1139.743	56.81	Sharp – right tail	-3.49	-2.60
1147.9	1137.5	3.8
1147.5	1137.0	3.8
943.4	934.8	0.0
940.5	932.0	0.0
937.0	928.5	0.0
907.7	899.5	1.2	916.76	68.52	Sharp	1.00	1.92
907.4	899.2	1.2
804.2	796.9	0.0
790.1	782.9	11.0
789.8	782.6	2.9
788.3	781.1	0.5	774.7743	55.99	Sharp	-1.72	-0.82
759.7	752.7	0.0
678.6	672.4	0.0	693.0542	76.3	Broad	2.14	3.07
677.8	671.6	0.0
609.5	604.0	0.0
595.8	590.4	6.1	590.8438	31.199	Sharp – right tail	-0.84	0.08
595.4	590.0	6.0	3401.148	82.81	Sharp	-5.62	-4.75
563.7	558.6	0.0	3325.696	81.18	Sharp – right tail	-7.71	-6.86

List of Symbols, Abbreviations, and Acronyms

2D	two-dimensional
ARL	Army Research Laboratory
ATR	attenuated total reflectance
COF	covalent organic framework
DCM	dichloromethane
DEVCOM	US Army Combat Capabilities Development Command
DFT	density functional theory
DMSO	dimethyl sulfoxide
Freq.	frequencies
FTIR	Fourier transform infrared
HDPE	high-density polyethylene
Inten.	intensities
IR	infrared
NAS	nucleophilic aromatic substitution
NMR	nuclear magnetic resonance
PXRD	powder X-ray diffraction
TABTCA	2,4,6-triaminobenzene-1,3,5-tricarboxyaldehyde
TGA	thermal gravimetric analysis

1 DEFENSE TECHNICAL
(PDF) INFORMATION CTR
DTIC OCA

1 DEVCOM ARL
(PDF) FCDD RLB CI
TECH LIB

2 DEVCOM ARL
(PDF) FCDD RLA MA
DC MCLEOD
FCDD RLB D
RH LAMBETH